

Supporting Information

## **A Hybrid-Ligand Exchange Strategy for High-Performance PbSe Quantum Dot Short-Wave Infrared Photodetectors**

Ya Wang,<sup>‡ab</sup> Min Chen,<sup>‡ab</sup> Manning Hu,<sup>a</sup> Anxin Jiao,<sup>a</sup> Faxin Wang,<sup>a</sup> Xiaolong Zheng,<sup>b</sup>  
Wanqing Li,<sup>a</sup> Xin Tang<sup>\*ab</sup> and Huicheng Hu<sup>\*a</sup>

<sup>‡</sup> The authors contributed equally to this article.

\* Corresponding author e-mail: xintang@bit.edu.cn; huichenghu@bitjx.edu.cn

a. Yangtze Delta Region Academy of Beijing Institute of Technology, Jiaxing 314019,  
People's Republic of China.

b. School of Optics and Photonics, Beijing Institute of Technology, Beijing 100081,  
People's Republic of China.

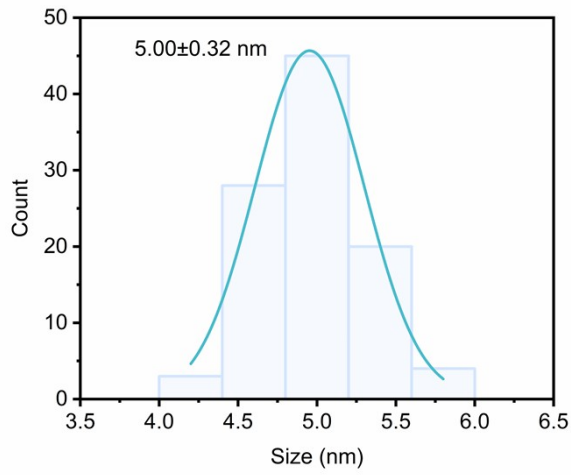


Figure S1. Size distribution histogram and Gaussian fitting curve of the PbSe CQDs.

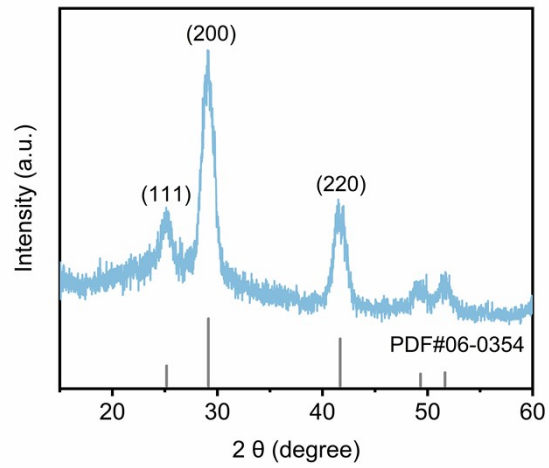


Figure S2. XRD pattern of the PbSe CQD film.

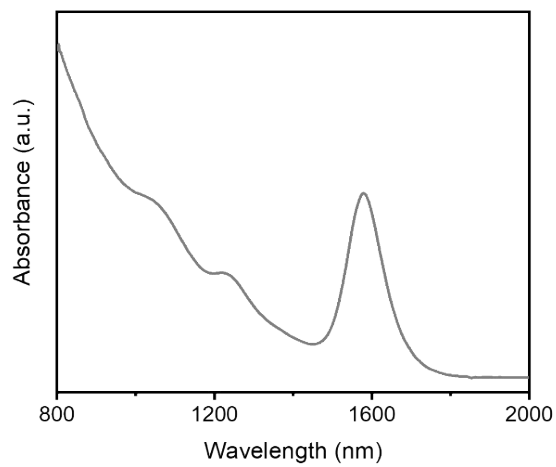


Figure S3. Absorption spectrum of the PbSe-OA film.

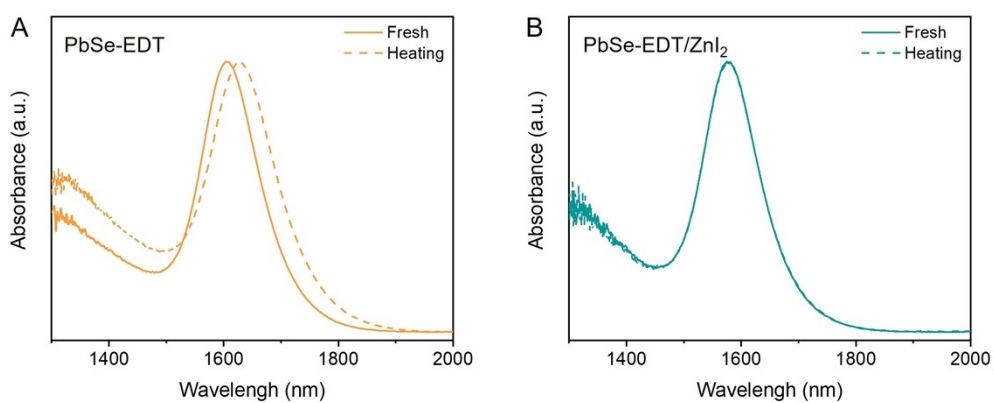


Figure S4. (A,B) Absorption spectra before and after heating treatment of the PbSe-EDT film (A) and PbSe-EDT/ZnI<sub>2</sub> film (B).

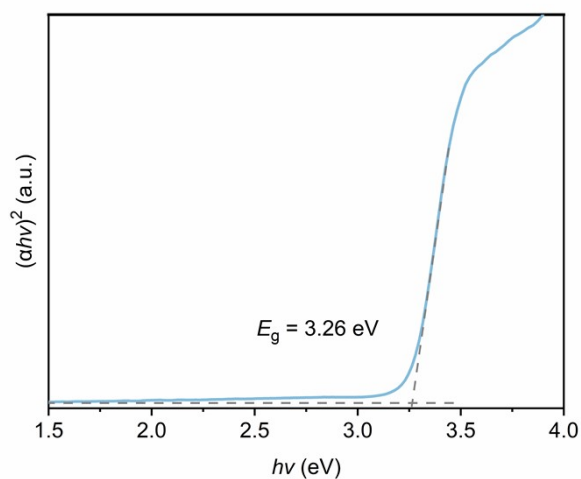


Figure S5. Tauc plots of the ZnO film.

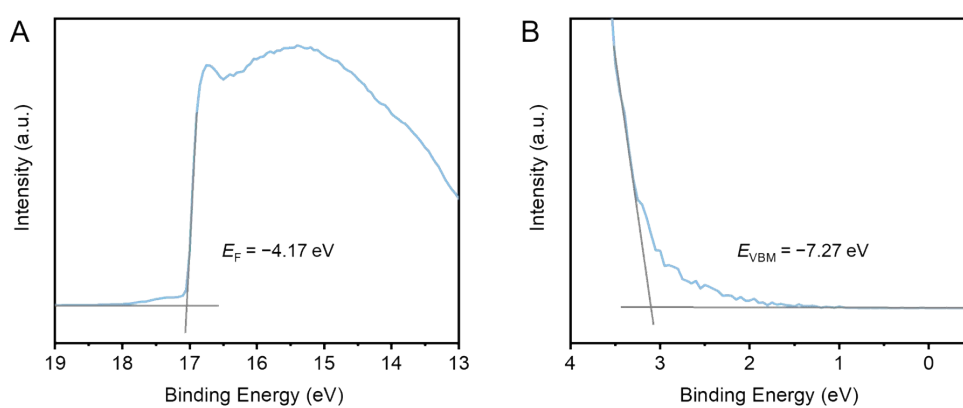


Figure S6. (A,B) UPS spectrum for determination of  $E_F$  (A) and energy difference between  $E_{VBM}$  and  $E_F$  (B) of ZnO film.

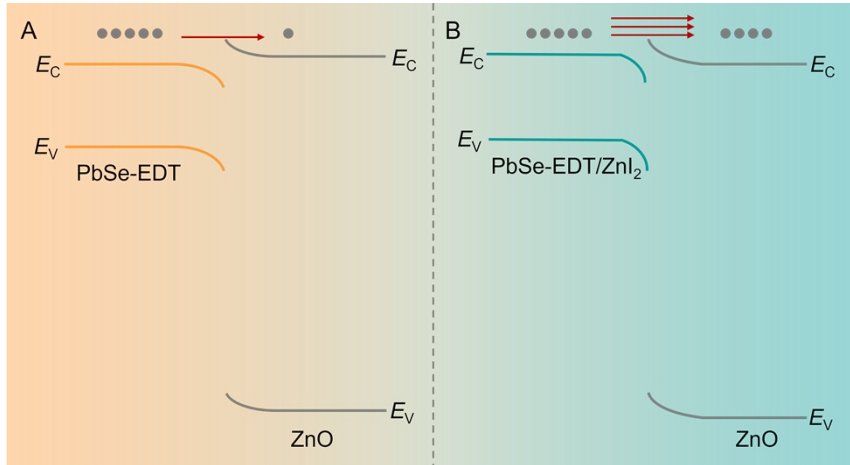


Figure S7. Schematic representation of carrier transport between PbSe CQD and ZnO films.

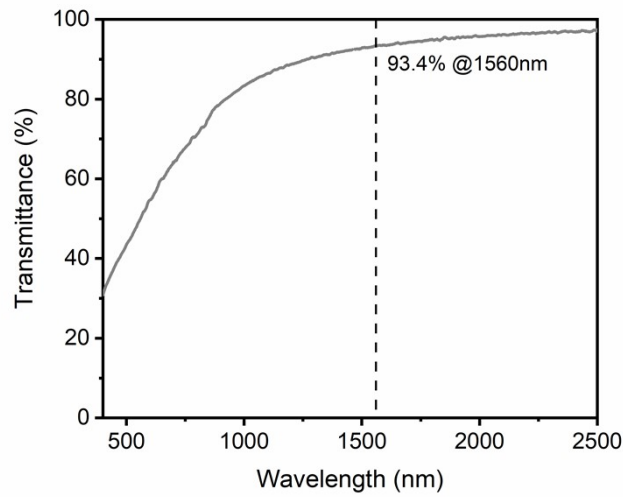


Figure S8. Transmittance spectrum of ZnTe film.

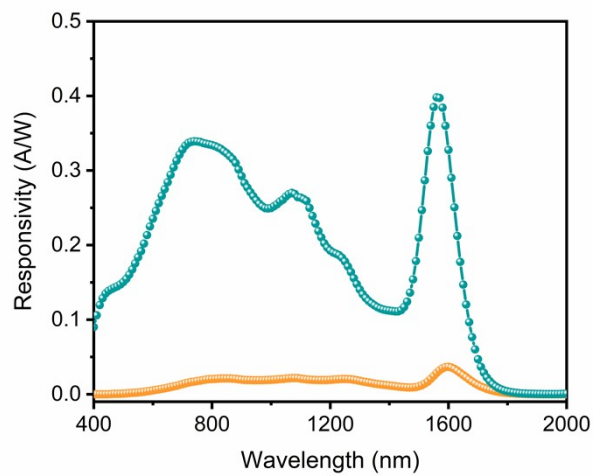


Figure S9. Broadband responsivity of PbSe-EDT and PbSe-EDT/ZnI<sub>2</sub> photodetectors.

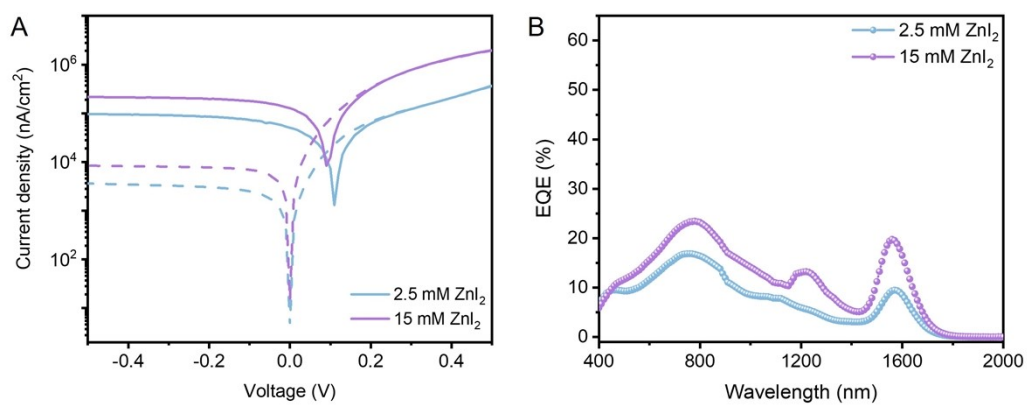


Figure S10. (A) The  $J$ - $V$  curves and (B) EQE spectra of PbSe-EDT/ZnI<sub>2</sub> photodetectors as the function of the concentration of ZnI<sub>2</sub>.

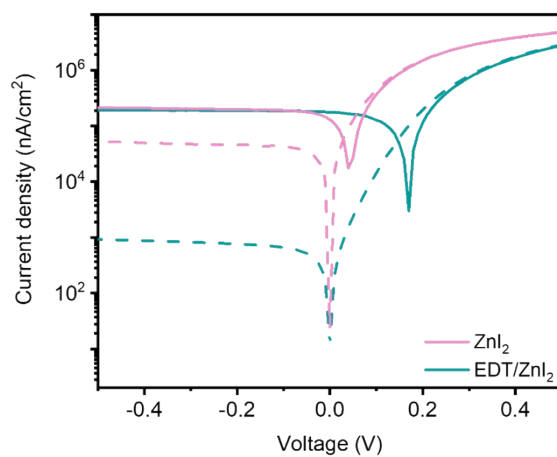


Figure S11. The  $J$ - $V$  curves of PbSe-ZnI<sub>2</sub> and PbSe-EDT/ZnI<sub>2</sub> photodetectors.

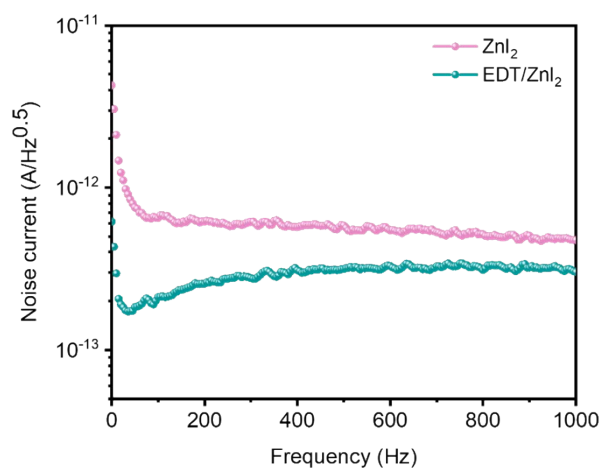


Figure S12. The noise spectral density of PbSe-ZnI<sub>2</sub> and PbSe-EDT/ZnI<sub>2</sub> photodetectors.

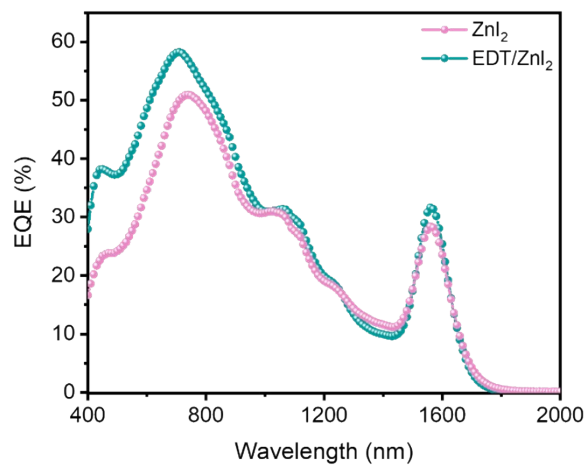


Figure S13. The EQE spectra of PbSe-ZnI<sub>2</sub> and PbSe-EDT/ZnI<sub>2</sub> photodetectors.

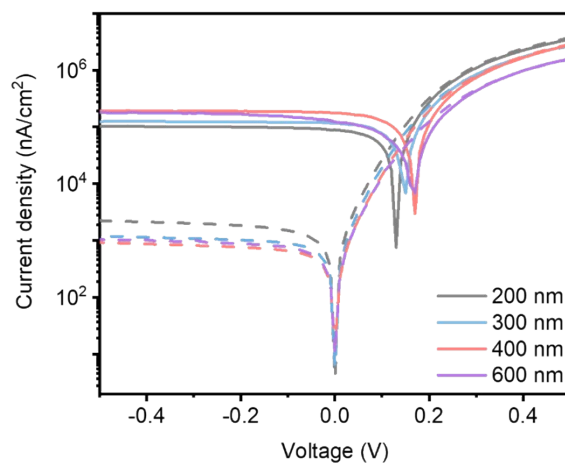


Figure S14. The  $J$ - $V$  curves of PbSe-EDT/ZnI<sub>2</sub> photodetectors as the function of absorption layer thickness.

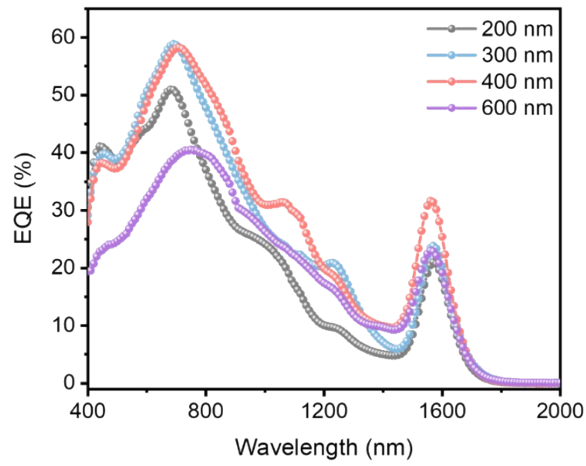


Figure S15. The EQE spectra of PbSe-EDT/ZnI<sub>2</sub> photodetectors as the function of absorption layer thickness.

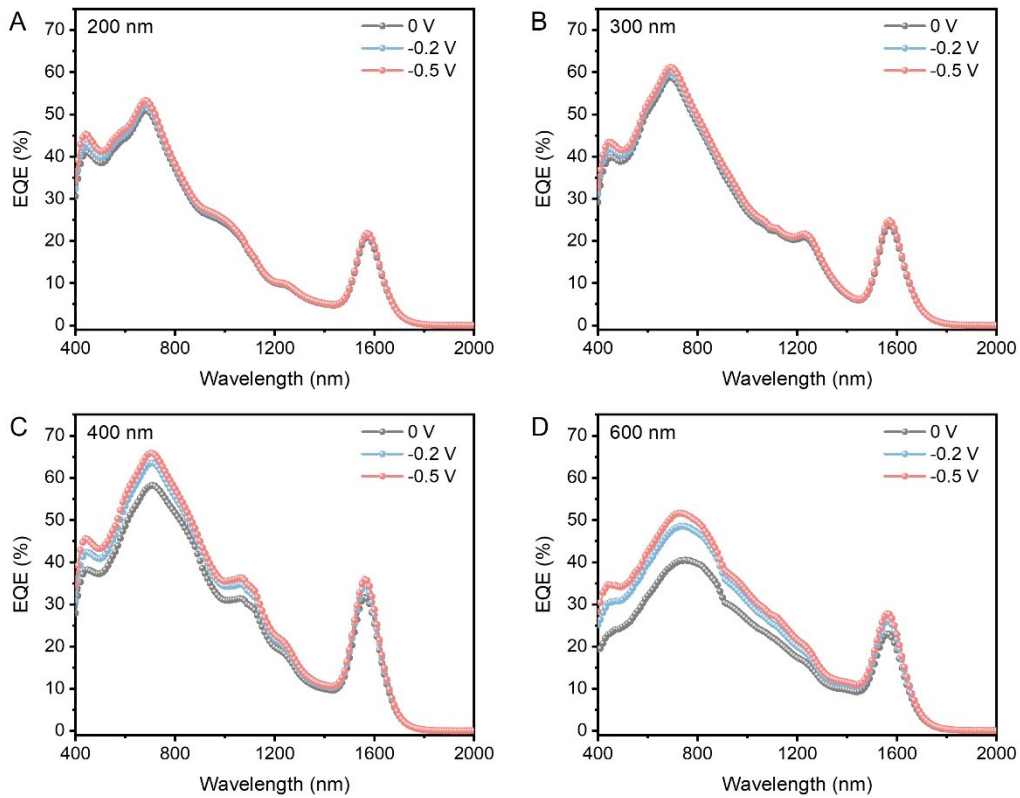


Figure S16. The EQE spectra of PbSe-EDT/ZnI<sub>2</sub> photodetectors under different bias voltages.

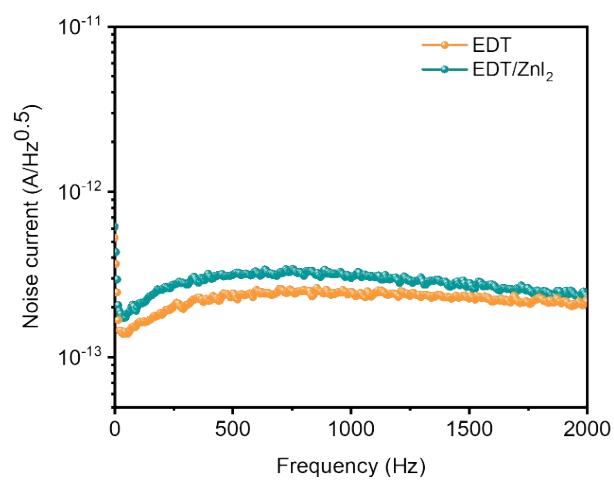


Figure S17. The noise spectral density of PbSe-EDT and PbSe-EDT/ZnI<sub>2</sub> photodetectors.

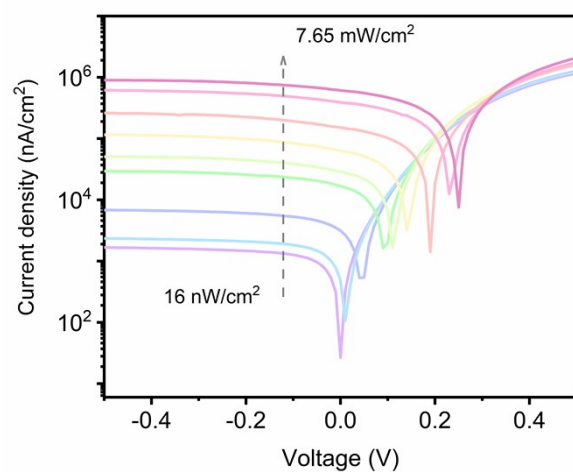


Figure S18. The  $J$ - $V$  curves of PbSe-EDT/ZnI<sub>2</sub> photodetector under 1550 nm illumination with different power density.

Table S1. The dark current density and EQE of PbSe-EDT/ZnI<sub>2</sub> photodetectors as the function of the concentration of ZnI<sub>2</sub>.

Concentration of ZnI <sub>2</sub> (mM)	Dark current density @-0.1 V (nA/cm <sup>2</sup> )	EQE (%)
0	2.2×10 <sup>3</sup>	2.8
2.5	3.6×10 <sup>3</sup>	9.5
10	9.2×10 <sup>2</sup>	31.4
15	8.4×10 <sup>3</sup>	19.8